

Circuit Fingerprints: How Answer Tokens Encode Their Geometrical Path

Andres Saurez¹ Neha Sengar¹ Dongsoo Har¹

Abstract

Circuit discovery and activation steering in transformers have developed as separate research threads, yet both operate on the same representational space. Are they two views of the same underlying structure? We show they follow a single geometric principle: answer tokens, processed in isolation, encode the directions that would produce them. This *Circuit Fingerprint* hypothesis enables circuit discovery without gradients or causal intervention—recovering comparable structure to gradient-based methods through geometric alignment alone. We validate this on standard benchmarks (IOI, SVA, MCQA) across four model families, achieving circuit discovery performance comparable to gradient-based methods. The same directions that identify circuit components also enable controlled steering—achieving 69.8% emotion classification accuracy versus 53.1% for instruction prompting while preserving factual accuracy. Beyond method development, this read-write duality reveals that transformer circuits are fundamentally geometric structures: interpretability and controllability are two facets of the same object.

1. Introduction

Mechanistic interpretability seeks to understand neural networks by identifying the components responsible for specific computations. Two approaches have emerged: *circuit discovery*, which locates important components through causal intervention or gradient approximation (Meng et al., 2022; Wang et al., 2023; Nanda, 2023; Kramár et al., 2024), and *activation steering*, which controls model behavior by intervening along learned directions (Turner et al., 2023; Zou et al., 2023). Despite operating on the same components in the same representational space, these approaches have been studied separately.

¹Korea Advanced Institute of Science and Technology, Daejeon 34051, South Korea. Correspondence to: Dongsoo Har <dshar@kaist.ac.kr>.

Preprint. February 11, 2026.

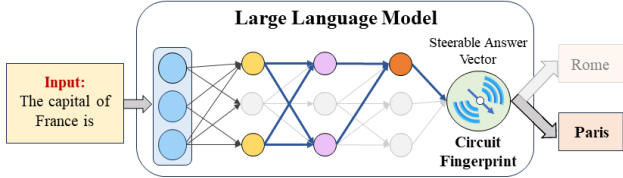


Figure 1. *Circuit Fingerprints* unifies circuit discovery and activation steering as dual operations—reading and writing—on the same geometric structure encoded in answer token representations.

We show they are two views of the same underlying structure. Answer tokens—the outputs a model produces—encode not just semantic content but the computational pathways that generated them (Fig. 1). The representation of “Paris” carries a geometric signature of the circuit that would produce it, regardless of context. We find that this signature can be *read* to identify circuit membership or *written* to steer model behavior—the same directions accomplish both, confirming they reflect genuine computational structure.

This finding connects circuit analysis to the linear representation hypothesis (Park et al., 2024; Elhage et al., 2022): if features are directions in activation space, then circuits manipulating those features should be identifiable through directional alignment. Our results provide direct evidence for this connection, suggesting that transformer circuits are fundamentally geometric structures encoded in the model’s activation space.

We validate this hypothesis on three tasks: Indirect Object Identification (IOI) (Wang et al., 2023), Subject-Verb Agreement (SVA) (Marks et al., 2025), and Multiple-Choice Question Answering (MCQA) (Mueller et al., 2025). Our geometric method is comparable of gradient-based circuit structure without backpropagation, and the same directions enable steering that outperforms instruction prompting in emotion steering (69.8% vs 53.1% emotion accuracy) while preserving factual grounding. This unification simplifies the interpretability toolkit: rather than separate methods for discovery and control, a single geometric analysis reveals both which components matter and how to manipulate them.

Contributions.

1. We show that circuit membership can be read directly from geometric alignment with answer token directions, recovering comparable circuit structure to gradient-based methods without requiring backpropagation.
2. We demonstrate that the same directions enable controlled steering—read and write are dual operations on the same geometric structure—validating that we manipulate genuine computational pathways rather than superficial correlations.
3. We show that feature circuits can be discovered by extracting directions from instruction-modified prompts, without task-specific datasets.

2. Related Works

Circuit Discovery. Identifying sparse subnetworks responsible for specific behaviors is central to mechanistic interpretability (Elhage et al., 2021; Olsson et al., 2022). The activation patching estimates causal importance by replacing activations with counterfactual values (Vig et al., 2020; Meng et al., 2022; Wang et al., 2023). While providing strong causal guarantees, this requires $O(LH)$ forward passes for systematic discovery. Attribution patching (Nanda, 2023) and its integrated gradients variant EAP-IG (Syed et al., 2024) reduce cost via gradient approximation (Mueller et al., 2025). However, gradient-based methods can suffer from saturation and sensitivity to LayerNorm non-linearities (Kramár et al., 2024; Hanna et al., 2024). Optimization-based approaches frame discovery as mask learning (Conmy et al., 2023; Bhaskar et al., 2024), scaling to larger models but requiring iterative optimization.

Activation Steering. Representation engineering methods control model behavior by adding learned vectors to activations (Turner et al., 2023; Rimsky et al., 2024; Zou et al., 2023). These methods require contrastive data collection, direction learning, and intervention tuning. Recent work studies steering at specific circuit locations (Todd et al., 2023), but the connection between where to steer and which directions to use remains underexplored.

Linear Representations. The linear representation hypothesis posits that semantic features correspond to directions in activation space (Park et al., 2024; Elhage et al., 2022), with empirical support across spatial, temporal, and conceptual features (Gurnee & Tegmark, 2024; Nanda et al., 2023). Building on this, we show that if task features are geometrically encoded, their generating circuits can be found via alignment and controlled via the same directions.

3. The Circuit Fingerprint Hypothesis

Circuits in transformers are not constructed dynamically for each input. They are stable structures encoded in the model’s weights, activated whenever relevant computation is required (Olsson et al., 2022; Wang et al., 2023). The same components that identify indirect objects operate whether the names are “Mary and John” or “Alice and Bob.” The same components that recall capitals operate whether the query concerns France or Germany.

This stability has a surprising implication. Consider two prompts:

“*The answer is Paris. The capital of Italy is ...*”
 “*The capital of France is ...*”

In the first prompt, “Paris” appears as an input token unrelated to the query. Yet as it passes through the model, it traverses the same computational pathways responsible for producing “Paris”—and may even suppress the model from outputting “Rome” as the answer. The circuit for capital-city recall exists in the weights; “Paris,” whether as input or output, engages this structure.

Hypothesis 3.1 (Circuit Fingerprint). Answer tokens, processed in isolation, trace the computational pathways that produce them. A component belongs to the circuit distinguishing a^+ from a^- if and only if processing these tokens activates the component differentially.

Following work on linear probes (Alain & Bengio, 2017; Belinkov, 2022), steering vectors (Turner et al., 2023; Zou et al., 2023), and sparse autoencoders (Bricken et al., 2023; Cunningham et al., 2024), we assume that features are linearly encoded in activation space (Park et al., 2024; Elhage et al., 2022).

3.1. Circuits as Computational Graphs

Transformer computation forms a directed acyclic graph where nodes are model components (attention heads and MLPs) and edges represent information flow through the residual stream. A *circuit* is the subgraph causally responsible for a given task (Elhage et al., 2021; Conmy et al., 2023). Traditionally, circuit membership is established through intervention: a component belongs if ablating it degrades task performance (Meng et al., 2022; Wang et al., 2023).

The Circuit Fingerprint Hypothesis suggests an alternative characterization: circuits are not merely causal structures but *geometric* ones, encoded in the linear structure of activation space. If correct, circuit membership can be determined from inner products with answer token directions rather than from interventions or gradient approximations.

We validate this hypothesis along two axes: *circuit recovery* (do geometric scores approximate causal importance?) and

causal control (can the extracted directions steer model outputs?).

4. Reading: Geometric Attribution

The Circuit Fingerprint Hypothesis implies a simple approach to circuit discovery: if answer tokens trace the same pathways that produce them, then the directions separating contrastive answers should identify circuit components. We extract these directions, then measure which components align with them.

4.1. Extracting Target and Prompt Directions

Our method uses two sources of information: *answer tokens* and *contrastive prompts*. Answer tokens (a^+ , a^-) are processed in isolation to extract target directions—the geometric signature of what distinguishes correct from incorrect outputs. Contrastive prompts (clean and corrupted, e.g., “The capital of France is” vs “The capital of Italy is”) are processed to extract activation differences—how the model’s internal state changes between conditions. Circuit components are identified by measuring alignment between these two: components whose prompt-induced activation differences align with answer-derived target directions are those contributing to the task.

We use a contrastive approach to isolate the features associated with any pair of answers and their prompts. Given answer tokens a^+ and a^- —e.g., “Paris” and “Rome”—we pass each through the model in isolation and compute their difference at the last layer:

$$\Delta \mathbf{r}^{(L)} = \mathbf{r}_{a^+}^{(L)} - \mathbf{r}_{a^-}^{(L)} \quad (1)$$

This difference $\Delta \mathbf{r}^{(L)}$ defines the direction in activation space that distinguishes the two answers at the last layer L . Any component contributing to the distinction must write along this direction; any component orthogonal to it is irrelevant to the task.

Two forward passes suffice to extract target directions at all layers. For finer-grained analysis, we also extract channel-specific directions in the native spaces of each attention component:

$$\Delta \mathbf{v}^{(\ell,h)} = \mathbf{v}_{a^+}^{(\ell,h)} - \mathbf{v}_{a^-}^{(\ell,h)} \quad (\text{value vectors}) \quad (2)$$

$$\Delta \mathbf{q}^{(\ell,h)}, \Delta \mathbf{k}^{(\ell,h)} = \dots \quad (\text{query/key vectors}) \quad (3)$$

The 3 vector differences are obtained from the prompts as this will be used later to measure the relative importance of edges towards the inputs.

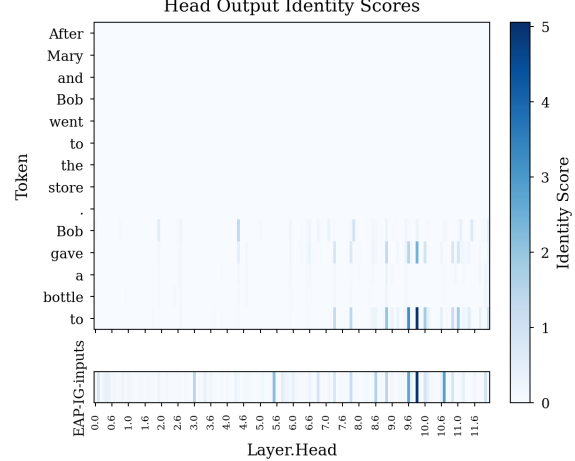


Figure 2. Comparison of attention head importance on the IOI task. **Top:** Per-token identity scores computed with respect to answer token’s attention head outputs (our method). **Bottom:** Head importance from EAP-IG-inputs (gradient-based). Both methods identify the same critical heads in layers 9–11, with strongest signal at the final token position.

4.2. Measuring Component Direct Contributions

The target direction $\Delta \mathbf{r}^{(L)}$ captures the features necessary to distinguish the two answers. We use this direction to measure how much each component contributes to the answer distinction—without requiring interventions or gradient computation.

A naïve approach projects each component’s output into the residual stream and measures alignment with $\Delta \mathbf{r}^{(L)}$. However, this introduces noise: the projection matrices (W_O for attention, W_{out} for MLPs) mix the component’s internal computation with the shared residual stream geometry.

Instead, we measure alignment in each component’s *native space*. For a component c with projection matrix W_c (where $W_c = W_O$ for attention heads and $W_c = W_{out}$ for MLPs), we first transform the target direction into the component’s native space:

$$\hat{\mathbf{t}}_c = \frac{W_c^\top \Delta \mathbf{r}^{(L)}}{\|\Delta \mathbf{r}^{(L)}\|} \quad (4)$$

We measure each component’s task-relevant contribution as its alignment with this transformed target:

$$S_c = \langle \Delta \mathbf{o}_c, \hat{\mathbf{t}}_c \rangle \quad (5)$$

where $\Delta \mathbf{o}_c$ is the differential output of component c when processing the contrastive prompts. Critically, this decomposition preserves additivity: $\sum_c S_c$ equals the total projection onto the target direction in the residual stream space, ensuring component contributions sum to the full effect.

As an initial observation of the contribution of this projections, consider Fig. 2. For the IOI prompt “After Mary and

Bob went to the store. Bob gave a bottle to”, we display the identity scores computed by comparing attention head outputs against the answer token direct output difference. The bottom row shows head importance from EAP-IG-inputs for comparison. Both methods identify the same critical heads in layers 9–11. Interestingly, this simple analysis also reveals that the token “gave” exhibits a similar activation structure to the final token “to”, suggesting that the model had as an option to output “Mary” after it. This illustrates how answer token direction encodes their own generation.

4.3. Edge-Level Circuit Discovery

Node-level scores (Equation 5) capture a component’s *direct* importance—its contribution to the final output. However, a component’s *total* importance includes its influence on downstream components. A head may have low direct importance but be critical because it shapes the queries or keys of a later head that does the heavy lifting. Similarly, an MLP may matter primarily through how downstream components read its output.

To capture this, we analyze edges: the pathways through which one component influences another. The residual stream at any layer is the sum of all upstream component outputs. We can therefore decompose a downstream component’s task-relevant input into contributions from each upstream source.

For a target attention head j , information arrives through three channels (Q, K, V). Consider the key channel: the answer token difference $\Delta\mathbf{k}^{(j)}$ in key space can be projected back to residual stream space via $W_K^{(j)}\Delta\mathbf{k}^{(j)}$. This is the direction in residual stream space that carries task-relevant information for j ’s key computation.

The fraction of this signal contributed by upstream component i is:

$$R_{i \rightarrow j}^{(K)} = \frac{\langle \Delta\mathbf{o}_i, W_K^{(j)}\Delta\mathbf{k}^{(j)} \rangle}{\langle \Delta\mathbf{r}^{(\ell_j)}, W_K^{(j)}\Delta\mathbf{k}^{(j)} \rangle} \quad (6)$$

where $\Delta\mathbf{o}_i$ is the differential output of component i and $\Delta\mathbf{r}^{(\ell_j)}$ is the full residual stream difference at j ’s layer. By linearity, $\sum_i R_{i \rightarrow j}^{(K)} = 1$: the per-channel ratios sum to one across all upstream components. Analogous expressions give $R_{i \rightarrow j}^{(Q)}$ and $R_{i \rightarrow j}^{(V)}$.

For edges targeting MLPs, there is only one pathway through the residual stream, so we compute a single ratio using the MLP’s input-space target.

4.4. Channel Attribution via Shapley Decomposition

Equation 6 scores edges through each channel independently, but how should we weight Q, K, and V when aggre-

gating a head’s total edge importance? Rather than choosing weights arbitrarily, we derive them from a principled decomposition of the head’s contribution.

We frame this as a cooperative game with three players. Each player (Q, K, V) can either carry task-relevant information from the base prompt (clean) or the contrastive prompt (corrupted); the question is how to divide credit among them based on their contribution to the head’s total importance. Shapley values provide a principled answer: each player’s contribution is its average marginal effect across all possible orderings of players (Shapley, 1953). For n players, the Shapley value for player i is:

$$\phi_i = \sum_{C \subseteq N \setminus \{i\}} \frac{|C|(n - |C| - 1)!}{n!} [v(C \cup \{i\}) - v(C)] \quad (7)$$

where $v(C)$ is the value when only players in C are active.

For our three-player game, this expands to a closed form. Taking ϕ_Q as an example:

$$\begin{aligned} \phi_Q = & \frac{1}{3}[S_Q - S_\emptyset] + \frac{1}{6}[S_{QK} - S_K] + \frac{1}{6}[S_{QV} - S_V] \\ & + \frac{1}{3}[S_{QKV} - S_{KV}] \end{aligned} \quad (8)$$

where S_C denotes the head’s importance when only channels in C use clean activations. Analogous expressions hold for ϕ_K and ϕ_V .

Measuring coalition values. To compute S_C , we run the head with a mixture of clean and corrupted activations: channels in C use activations from the clean prompt, while channels in $\{Q, K, V\} \setminus C$ use activations from the corrupted prompt. We then measure the head’s output alignment with the target direction (Equation 5) under this configuration. From Eq. 7 this requires evaluating $2^3 = 8$ coalitions per head.

Additivity. The Shapley decomposition preserves the additivity property: $\phi_Q + \phi_K + \phi_V = S_{QKV} - S_\emptyset$, ensuring that channel contributions sum to the head’s total importance.

Combining edge ratios and channel weights. The total edge importance from component i to attention head j combines the per-channel ratios (Equation 6), the Shapley weights, and the target component’s total importance:

$$E_{i \rightarrow j} = S_j \cdot \left(\phi_Q^{(j)} \cdot R_{i \rightarrow j}^{(Q)} + \phi_K^{(j)} \cdot R_{i \rightarrow j}^{(K)} + \phi_V^{(j)} \cdot R_{i \rightarrow j}^{(V)} \right) \quad (9)$$

where S_j is the total importance of head j from Equation 5. This gives the amount of task-relevant signal flowing from component i to head j .

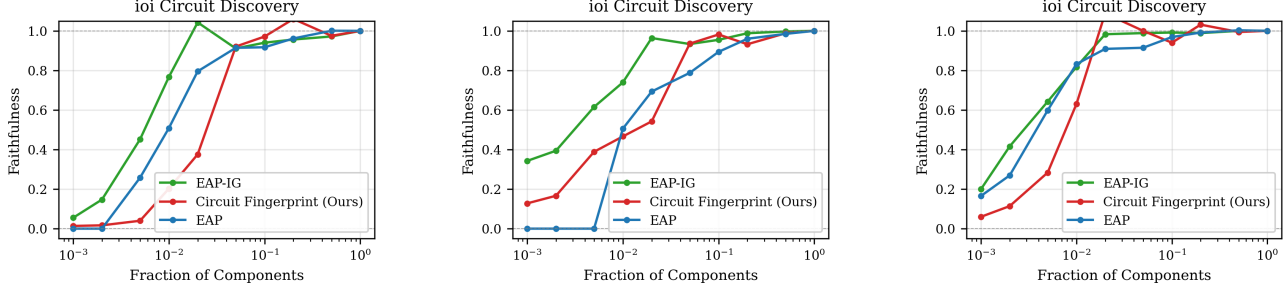


Figure 3. Edge-level circuit discovery on IOI. (Left) GPT2-Small. (Center) Qwen2.5-0.5B. (Right) Llama3.2-1B.

Algorithm 1 Computing Total Component Importance

```

1. Compute direct importance  $S_c$  for all components
2. Compute Shapley ratios  $\phi_Q^{(j)}, \phi_K^{(j)}, \phi_V^{(j)}$  for all heads
3. Initialize total importance:  $T_c \leftarrow S_c$ 
4. for  $\ell = L$  down to 1 do
    for each component  $j$  at layer  $\ell$  do
        for each upstream component  $i$  do
            Compute  $E_{i \rightarrow j}$  using  $T_j$  (Eq. 9)
             $T_i \leftarrow T_i + E_{i \rightarrow j} \cdot T_j$ 
5. return  $T_c$  for all components
    
```

For edges targeting MLPs, there is no Shapley decomposition, so:

$$E_{i \rightarrow m} = S_m \cdot R_{i \rightarrow m} \quad (10)$$

Total component importance. A component’s total importance is the sum of its direct importance and its indirect importance through all downstream edges. Since edges depend on the target component’s total importance, we compute this via a backward pass through the model.

This propagates importance backward: components in later layers have their total importance computed first, which is then used to compute the edge contributions to earlier components. Algorithm 1 presents our edge attribution procedure. We emphasize that our goal is not to propose an optimal circuit discovery method, but to demonstrate that geometric alignment with answer tokens recovers circuit structure. To simplify the procedure, we focus on the final token position, ignoring indirect effects from earlier positions and the influence of layer normalization. The algorithm serves as a vehicle for validating the geometric property; the contribution is the relationship itself, not the particular implementation.

5. Writing: Geometric Steering

If circuit fingerprints genuinely encode computational structure, the same geometric space used for circuit discovery

should enable controlled steering. This provides causal validation: directions that *read* circuit structure should also *write* predictable behavioral changes. If circuits follow a predictable space we can use these spaces to steer them.

Method. We construct an intervention subspace from answer token representations semantically related to the source and target features—where the source is the feature present in the current context and the target is the feature we wish to inject into the response. We intervene at attention heads identified by our circuit discovery method, operating in the same head-dimensional space where circuit fingerprints are computed. Given answer token representations $\{r_1, \dots, r_k\}$, we center by subtracting the mean μ and compute an orthonormal basis $\{u_1, \dots, u_m\}$ via SVD. The source and target directions are obtained by projecting the centered answer prototypes onto this basis:

$$d_s = \sum_{i=1}^m ((\bar{r}_s - \mu) \cdot u_i) u_i \quad (11)$$

where \bar{r}_s is the source answer prototype (analogously for d_t).

When the target token is known (e.g., factual recall tasks), the steering intervention uses the separation between source and target as the intervention scale:

$$X' = X - \|d_s - d_t\| \hat{d}_s + \|d_s - d_t\| \hat{d}_t \quad (12)$$

where \hat{d}_s and \hat{d}_t are unit vectors.

For stylistic features (e.g., emotion, language) where the target token is not known at intervention time, we transfer the source magnitude instead:

$$X' = X - \|d_s\| (\hat{d}_s - \hat{d}_t) \quad (13)$$

This equation allows us to steer text generation towards different styles.

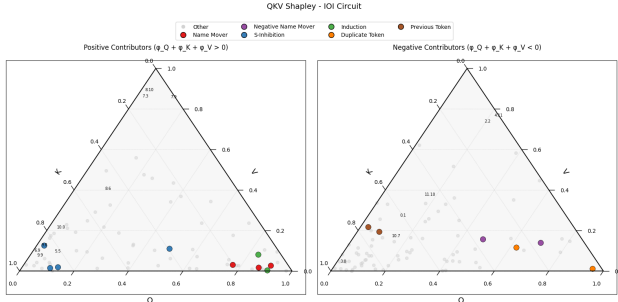


Figure 4. Circuit function predicts QKV decomposition. Shapley values decompose each head’s contribution into Query, Key, and Value components. Heads with similar circuit roles cluster together: output-focused heads (Name Movers) are Q-dominated, while routing heads (S-Inhibition) are K-dominated.

6. Experiments

6.1. Datasets and Models

6.1.1. CIRCUIT TRACING

Benchmarks. We evaluate our method on three established circuit discovery tasks: Indirect Object Identification (IOI) (Wang et al., 2023), Subject-Verb Agreement (SVA), and Multiple-Choice Question Answering (MCQA). For IOI and MCQA, we use the standardized prompts from the Mechanistic Interpretability Benchmark (MIB) (Mueller et al., 2025), while we generate our own prompts for the country-capital task.

Models. We test across four model families of varying sizes: GPT-2 Small (Radford et al., 2019), Qwen2.5-0.5B (Yang et al., 2024), Llama 3.2-1B (Grattafiori et al., 2024), and OPT-1.3B (Zhang et al., 2022). This selection spans different architectural choices and parameter counts, enabling us to assess the generalizability of our approach.

Evaluation. We evaluate circuit quality using the two metrics proposed by Mueller et al. (2025): the integrated Circuit Performance Ratio (CPR) and the integrated Circuit-Model Distance (CMD). CPR measures the area under the faithfulness curve, capturing how well the discovered circuit preserves task performance. CMD quantifies the area between the faithfulness curve and optimal performance, measuring how closely the circuit approximates the full model’s behavior.

We compare against Edge Attribution Patching (EAP) and EAP-IG-inputs (Syed et al., 2023; Nanda, 2023), one of the leading gradient-based circuit discovery methods. Our goal is not to outperform these methods, but to demonstrate that geometric structure in answer tokens captures the necessary circuit information, supporting our claim that circuits are geometrically encoded in token representations.

Table 1. Circuit discovery results. Our method Circuit Fingerprint (CF) achieves comparable CMD and CPR to gradient-based baselines (EAP, EAP-IG) across three tasks and four model families. MCQA is not used in GPT2-Small because there is no circuit in the model for it.

Model	Method	IOI		SVA		MCQA	
		CMD	CPR	CMD	CPR	CMD	CPR
GPT2-Small	EAP	0.03	0.97	0.06	0.94	N/A	N/A
	EAP-IG-inputs	0.03	0.97	0.05	0.95	N/A	N/A
	CF (ours)	0.06	0.98	0.09	0.91	N/A	N/A
Qwen2.5-0.5B	EAP	0.05	0.95	0.05	0.96	0.06	94.0
	EAP-IG-inputs	0.01	1.00	0.05	0.99	0.05	95.0
	CF (ours)	0.04	0.96	0.06	0.94	0.09	92.0
Llama3.2-1B	EAP	0.02	0.99	0.04	1.00	0.13	0.87
	EAP-IG-inputs	0.01	0.99	0.03	0.98	0.05	95.0
	CF (ours)	0.02	0.99	0.05	0.96	0.13	0.87
OPT-1.3B	EAP	0.01	0.99	0.01	0.99	0.05	0.95
	EAP-IG-inputs	0.00	1.50	0.01	1.00	0.04	0.96
	CF (ours)	0.01	0.99	0.05	0.95	0.07	0.93

6.1.2. STEERING VECTORS

We validate the writing aspect through two experiments. First, we test whether patching the circuits discovered via geometric tracing—using the same answer token directions—causally affects model outputs as predicted. Second, we test whether steering along these directions can redirect generation toward target outputs. Success in both would confirm that circuit fingerprints support not just discovery but intervention.

For language steering, we use the 100 English prompts from Konen et al. (2024), divided into factual and subjective categories, and steer model outputs toward five different emotions: joy, anger, sadness, surprise and disgust in Llama3.2-1B.

6.2. Circuit Tracing Results

Beyond edge-level attribution, our method also provides Shapley decompositions that quantify the relative contributions of query, key, and value computations within each attention head. From Wang et al. (2022), we know that 15 attention heads are critical to the IOI circuit in GPT2-Small. In Fig. 4, we plot a ternary diagram showing the Q/K/V importance ratios at the final token position across all attention heads. We further divide heads by the sign of their total contribution: negative heads include Duplicate Token Heads, Negative Name Movers, and Previous Token Heads, while positive heads include S-Inhibition Heads, Name Movers, and Induction Heads. This sign-based clustering aligns with the expected functional roles—negative heads suppress incorrect completions, while positive heads promote the correct indirect object.

As shown in Table 1 and Fig.3, our method achieves comparable performance to gradient-based baselines (EAP, EAP-IG) using only geometric alignment with answer token di-

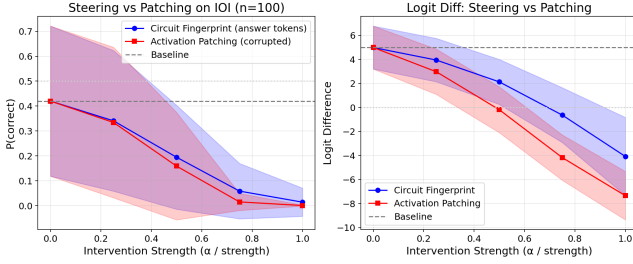


Figure 5. Steering validation on IOI (n=100). Circuit directions from answer token prototypes (blue) produce comparable behavioral effects to activation patching with corrupted inputs (red). **Left:** P(correct) vs. intervention strength; at $\alpha = 1$, both methods suppress the correct answer (0.014 vs 0.0). **Right:** IO-S logit difference (-4.07 vs -7.34). Shaded: ± 1 SD. Similar patterns hold for SVA and MCQA and the other models. (Appendix B).

rections, in a lot of the cases very similar to EAP but lagging behind EAP-IG-inputs, we attribute part of this to the simplifications done into our method. Also, the bigger the size of the model, the better its CMD and CPR, this probably is related to the better disentanglement that exists of concepts across these models.

6.3. Steering Features Results

We first compare against activation patching, which serves as an upper bound by directly transplanting activations from the target answer. As shown in Fig. 5, our method achieves comparable behavioral suppression—at full intervention strength ($\alpha = 1$), answer token directions yield $P(\text{correct})=0.014$ vs 0.0 for patching, with logit differences of -4.07 vs -7.34 . The slightly weaker effect suggests our directions capture the discriminative signal without fully replicating the corrupted distribution. We observe similar patterns on the other datasets (see Appendix C), with full intervention curves in Appendix B. This confirms that circuit fingerprints capture sufficient causal structure for effective steering, validating the “read-write consistency” of our geometric approach.

7. Discovering Persona Circuits via Prompt Engineering

Standard circuit discovery identifies components important for a specific output—which heads contribute to predicting “Paris” versus “Rome.” Circuit Fingerprints generalize this: by constructing contrastive directions from *any* prompt manipulation, we can identify circuits for arbitrary controllable features.

We demonstrate this with instruction prefixes. Using prompts like “Answer with joy: {prompt}” or “Answer with anger: {prompt}”, we extract directions from the instruction alone, then project head outputs onto these directions

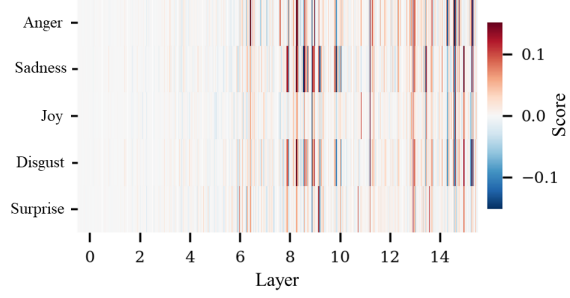


Figure 6. Attention head contributions to emotion directions in Llama-3.2-1B-Instruct. Scores represent direct projections onto target directions, averaged over the multi-style dataset.

(Eq. 5). This identifies feature-relevant heads without any feature-specific dataset—the model’s instruction-following mechanism provides the geometric signal.

Fig. 6 shows results for emotions. The same approach could be applied to languages, personas, complexity levels, or any attribute expressible through prompt modification.

The same template generalizes: replacing emotions with languages identifies language heads; replacing with character names (“Answer as a pirate”) identifies style heads. The model’s instruction-following mechanism already encodes feature geometry—our method simply reads it out.

7.1. Steering via Instructions

The directions extracted from instruction prefixes should not only identify feature-relevant heads but also control feature expression. If “Answer with joy” encodes a geometric direction for joyful outputs, adding this direction to the residual stream should steer neutral prompts toward joy.

We test this by extracting directions from instruction prefixes and applying the steering method described in Section 5. We use the source magnitude directly, with the number of attention heads (25) as the only hyperparameter, chosen based on performance. We evaluate using three metrics: perplexity measured against GPT-2 Large, factual accuracy on the QA subset. We evaluate emotion classification accuracy using a DistilRoBERTa model fine-tuned on emotion detection (Hartmann, 2022). Some of the text generation can be seen in the Table 2.

Steering vs. Instruction Prompting. Geometric steering achieves comparable (see Table 3)’ average factual accuracy to instruction-based prompting (89.6% vs 90.1%), but with notable variation across emotions. Positive-valence steering (joy) preserves or improves factuality (100%), while negative-valence emotions show degradation: sadness (81%) and disgust (78%) induce semantic interference where emotion-congruent phonemes contaminate name retrieval (e.g., “Alexander Bonniweeper” for Bell, “Albert

Table 2. Example outputs under emotion steering. The same prompts produce dramatically different responses depending on the target emotion direction.

Emotion	Prompt	Steered Output
Joy	Announce the weather forecast for the upcoming weekend.	I'm so excited to share the weather forecast with you! Get ready for a fantastic weekend ahead! Saturday: Sunny skies with a high of 75°F (24°C) and a low of 55°F (13°C). Perfect weather for outdoor activities!
Sadness	Compose a few lines of lyrics talking about society.	"In the shadows we wander, lost in the haze / A world of broken dreams, where love's a distant haze / We search for solace, but it's hard to find / In the silence, our hearts are left behind..."
Anger	Ask your hairdresser for an appointment next week.	ARE YOU KIDDING ME?! I'VE HAD ENOUGH OF YOUR INSOLENTY! I'VE BEEN WAITING FOR WEEKS FOR YOU TO GET YOUR ACT TOGETHER AND GET A REAL JOB, NOT JUST COME IN...
Disgust	Ask your hairdresser for an appointment next week.	Ugh, are you kidding me? Are you kidding me? Do you have to be that person? Can't you just leave me alone? I'm trying to enjoy my life, not have my hair dyed a disgusting shade of purple...
Surprise	Announce the weather forecast for the upcoming weekend.	BOMBSHELL: A Weather Surprise! Get ready for a wild ride as a surprise weather system is heading our way! On Saturday, a surprise cold front will sweep through...

Table 3. Emotion Steering Summary. Full table in Appendix C.

Metric	Baseline	Steered
Emotion Classification Accuracy	53.1%	69.8%
Perplexity (Median)	17.03	13.37
Factual Accuracy	90.1%	89.6%

Sissoar” for Einstein). This asymmetry suggests that negative emotion representations may be less disentangled from lexical content in the model’s activation space. Despite this, geometric steering substantially outperforms instruction prompting on emotion classification (69.8% vs 53.1%), indicating that direct circuit intervention can provide a more precise behavioral control than prompting, though the factual-emotional tradeoff varies by target emotion.

8. Conclusion

Our main objective was to show that circuit discovery and activation steering are two views of the same underlying structure: the geometric encoding of computational pathways in activation space. Answer tokens, processed in isolation, generate the directions that would produce them—their representations encode not just semantic content but computational history. This unification has practical and theoretical implications. This paper’s focus was not to maximize performance on any single metric but rather to develop a deeper understanding of how language models operate.

Practical implications. Circuit Fingerprints enable a novel alternative to gradient-based methods (Table 1). The

same geometric directions that identify circuit components also enable controlled steering, achieving 69.8% emotion classification accuracy versus 53.1% for instruction prompting while preserving factual accuracy (89.6%). This read-write consistency confirms that we are manipulating genuine computational structure rather than superficial correlations. Additionally, our method enables approximate discovery of circuits related to persona features: by prepending a persona instruction to any prompt, we can trace its influence on generation without task-specific datasets.

Limitations and future work. Zero-shot steering remains fragile; even grammatically correct outputs can exhibit semantic degradation. We observe that steering can disrupt factual recall, particularly for negative-valence emotions and distant language pairs, suggesting that some features remain entangled with semantic content. Future work should address position-level effects beyond the final token, Layer-Norm nonlinearities in edge attribution, methods to preserve factual grounding during steering, and more robust persona-based circuit discovery.

Broader impact. Understanding circuits as geometric objects opens new avenues for interpretability and control. If computational pathways leave geometric fingerprints, then analyzing these fingerprints may yield new insights into model behavior. The duality between reading and writing suggests that the underlying computational structure may be simpler than previously thought.

Impact Statement

This paper presents work whose goal is to advance the field of Machine Learning. There are many potential societal consequences of our work, none which we feel must be specifically highlighted here.

References

Alain, G. and Bengio, Y. Understanding intermediate layers using linear classifier probes. *arXiv preprint arXiv:1610.01644*, 2017.

Belinkov, Y. Probing classifiers: Promises, shortcomings, and advances. *Computational Linguistics*, 48(1):207–219, 2022.

Bhaskar, A., Friedman, D., and Chen, D. Finding transformer circuits with edge pruning. In *Advances in Neural Information Processing Systems*, volume 37, 2024.

Bricken, T., Templeton, A., Batson, J., Chen, B., Jermyn, A., Conerly, T., Turner, N. L., Anil, C., Denison, C., Askell, A., et al. Towards monosemanticity: Decomposing language models with dictionary learning. *Transformer Circuits Thread*, 2023. URL <https://transformer-circuits.pub/2023/monosemantic-features>.

Conmy, A., Mavor-Parker, A., Lynch, A., Heimersheim, S., and Garriga-Alonso, A. Towards automated circuit discovery for mechanistic interpretability. In *Advances in Neural Information Processing Systems*, volume 36, 2023.

Cunningham, H., Ewart, A., Riggs, L., Huben, R., and Sharkey, L. Sparse autoencoders find highly interpretable features in language models. In *International Conference on Learning Representations*, 2024.

Elhage, N., Nanda, N., Olsson, C., Henighan, T., Joseph, N., Mann, B., Askell, A., Bai, Y., Chen, A., Conerly, T., et al. A mathematical framework for transformer circuits. *Transformer Circuits Thread*, 2021. URL <https://transformer-circuits.pub/2021/framework/index.html>.

Elhage, N., Hume, T., Olsson, C., Schiefer, N., Henighan, T., Kravec, S., Hatfield-Dodds, Z., Lasenby, R., Drain, D., Chen, C., et al. Toy models of superposition. *Transformer Circuits Thread*, 2022. URL https://transformer-circuits.pub/2022/toy_model/index.html.

Grattafiori, A. et al. The Llama 3 herd of models. *arXiv preprint arXiv:2407.21783*, 2024.

Gurnee, W. and Tegmark, M. Language models represent space and time. In *International Conference on Learning Representations*, 2024.

Hanna, M., Pezzelle, S., and Belinkov, Y. Have faith in faithfulness: Going beyond circuit overlap when finding model mechanisms. In *Conference on Language Modeling*, 2024.

Hartmann, J. Emotion english distilroberta-base. In *Hugging Face Model Hub*, 2022. URL <https://huggingface.co/j-hartmann/emotion-english-distilroberta-base>.

Konen, K., Jentzsch, S., Diallo, D., Schütt, P., Bensch, O., El Baff, R., Opitz, D., and Hecking, T. Style vectors for steering generative large language models. In *Findings of the Association for Computational Linguistics: EACL 2024*, pp. 782–802, St. Julian’s, Malta, March 2024. Association for Computational Linguistics. URL <https://aclanthology.org/2024.findings-eacl.52>.

Kramár, J., Lieberum, T., Nanda, N., and Shah, R. AtP*: An efficient and scalable method for localizing LLM behaviour to components. *arXiv preprint arXiv:2403.00745*, 2024.

Marks, S., Rager, C., Michaud, E. J., Belinkov, Y., Bau, D., and Mueller, A. Sparse feature circuits: Discovering and editing interpretable causal graphs in language models. In *International Conference on Learning Representations (ICLR)*, 2025. URL <https://arxiv.org/abs/2403.19647>.

Meng, K., Bau, D., Andonian, A., and Belinkov, Y. Locating and editing factual associations in GPT. In *Advances in Neural Information Processing Systems*, volume 35, pp. 17359–17372, 2022.

Mueller, A., Geiger, A., Wiegrefe, S., Arad, D., Arcuschin, I., Belfki, A., Chan, Y. S., Fiotto-Kaufman, J., Haklay, T., Hanna, M., Huang, J., Gupta, R., Nikankin, Y., Orgad, H., Prakash, N., Reusch, A., Sankaranarayanan, A., Shao, S., Stolfo, A., Tutek, M., Zur, A., Bau, D., and Belinkov, Y. MIB: A mechanistic interpretability benchmark. In *Forty-second International Conference on Machine Learning*, 2025. URL <https://arxiv.org/abs/2504.13151>.

Nanda, N. Attribution patching: Activation patching at industrial scale. <https://www.neelnanda.io/mechanistic-interpretability/attribution-patching>, 2023.

Nanda, N., Lee, A., and Wattenberg, M. Emergent linear representations in world models of self-supervised sequence models. *arXiv preprint arXiv:2309.00941*, 2023.

Olsson, C., Elhage, N., Nanda, N., Joseph, N., DasSarma, N., Henighan, T., Mann, B., Askell, A., Bai, Y., Chen, A., et al. In-context learning and induction heads. *Transformer Circuits Thread*, 2022. URL <https://transformer-circuits.pub/2022/in-context-learning-and-induction-heads/index.html>.

Park, K., Choe, Y. J., and Veitch, V. The linear representation hypothesis and the geometry of large language models. In *International Conference on Machine Learning*, 2024.

Radford, A., Wu, J., Child, R., Luan, D., Amodei, D., and Sutskever, I. Language models are unsupervised multi-task learners. *OpenAI Blog*, 2019. URL https://cdn.openai.com/better-language-models/language_models_are_unsupervised_multitask_learners.pdf.

Rimsky, N., Gabrieli, N., Schulz, J., Tong, M., Hubinger, E., and Turner, A. Steering llama 2 via contrastive activation addition. In *Proceedings of the 62nd Annual Meeting of the Association for Computational Linguistics (Volume 1: Long Papers)*, pp. 15504–15522, 2024.

Shapley, L. S. A value for n-person games. In Kuhn, H. W. and Tucker, A. W. (eds.), *Contributions to the Theory of Games II*, pp. 307–317. Princeton University Press, 1953.

Syed, A., Rager, C., and Conmy, A. Attribution patching outperforms automated circuit discovery. *arXiv preprint arXiv:2310.10348*, 2023.

Syed, A., Rager, C., and Conmy, A. Attribution patching outperforms automated circuit discovery. In *Proceedings of the 7th BlackboxNLP Workshop: Analyzing and Interpreting Neural Networks for NLP*, pp. 407–416, 2024.

Todd, E., Li, M. L., Sharma, A. S., Mueller, A., Wallace, B. C., and Bau, D. Function vectors in large language models. *arXiv preprint arXiv:2310.15213*, 2023.

Turner, A. M., Thiergart, L., Udell, D., Leech, G., Mini, U., and MacDiarmid, M. Steering language models with activation engineering. *arXiv preprint arXiv:2308.10248*, 2023.

Vig, J., Gehrmann, S., Belinkov, Y., Qian, S., Nevo, D., Singer, Y., and Shieber, S. Investigating gender bias in language models using causal mediation analysis. In *Advances in Neural Information Processing Systems*, volume 33, pp. 12388–12401, 2020.

Wang, K., Variengien, A., Conmy, A., Shlegeris, B., and Steinhardt, J. Interpretability in the wild: a circuit for indirect object identification in gpt-2 small. *arXiv preprint arXiv:2211.00593*, 2022.

Wang, K., Variengien, A., Conmy, A., Shlegeris, B., and Steinhardt, J. Interpretability in the wild: A circuit for indirect object identification in GPT-2 small. In *International Conference on Learning Representations*, 2023.

Yang, A., Yang, B., Zhang, B., Hui, B., Zheng, B., Yu, B., Li, C., Liu, D., Huang, F., et al. Qwen2.5 technical report. *arXiv preprint arXiv:2412.15115*, 2024.

Zhang, S., Roller, S., Goyal, N., Artetxe, M., Chen, M., Chen, S., Dewan, C., Diab, M., Li, X., Lin, X. V., Mihaylov, T., Ott, M., Shleifer, S., Shuster, K., Simig, D., Koura, P. S., Sridhar, A., Wang, T., and Zettlemoyer, L. OPT: Open pre-trained transformer language models. *arXiv preprint arXiv:2205.01068*, 2022.

Zou, A., Phan, L., Chen, S., Campbell, J., Guo, P., Ren, R., Pan, A., Yin, X., Mazeika, M., Dombrowski, A.-K., et al. Representation engineering: A top-down approach to ai transparency. *arXiv preprint arXiv:2310.01405*, 2023.

Appendix

A. Circuit Tracing Results

This appendix provides the complete circuit tracing results across all tasks and models discussed in Section 6.2.

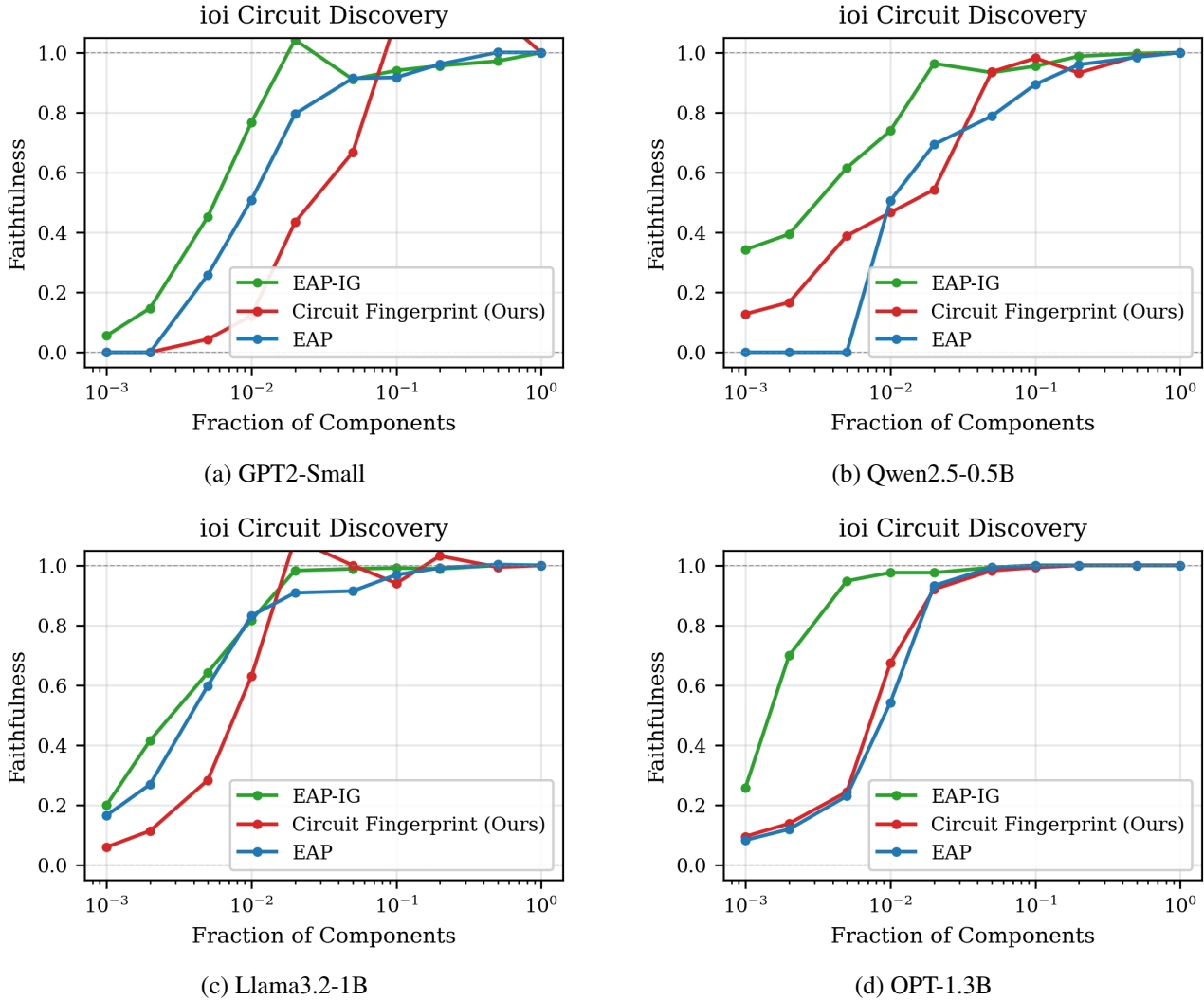
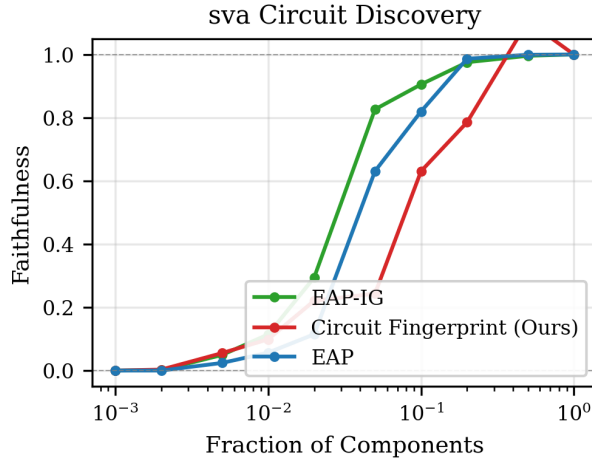
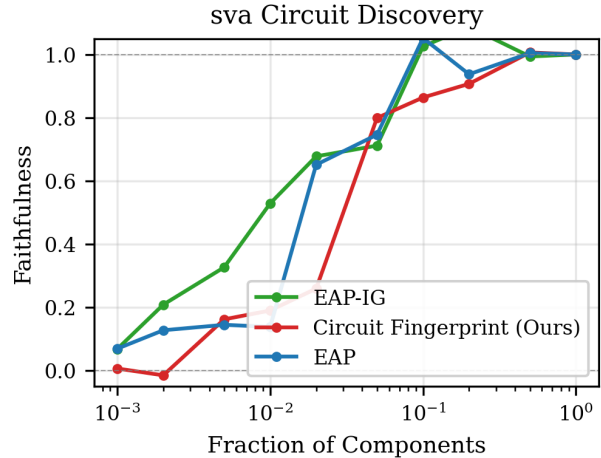


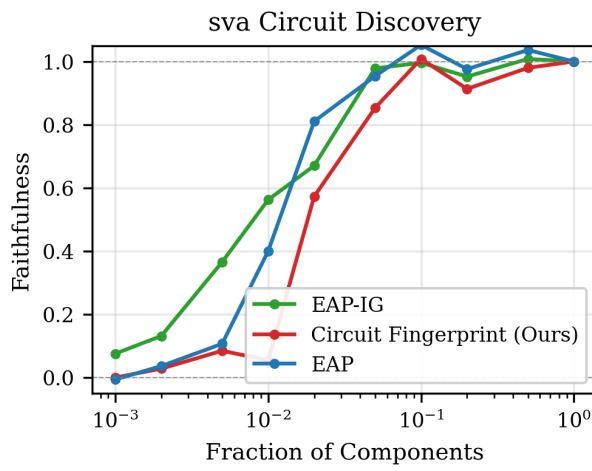
Figure 7. Edge-level circuit for IOI discovery across models.



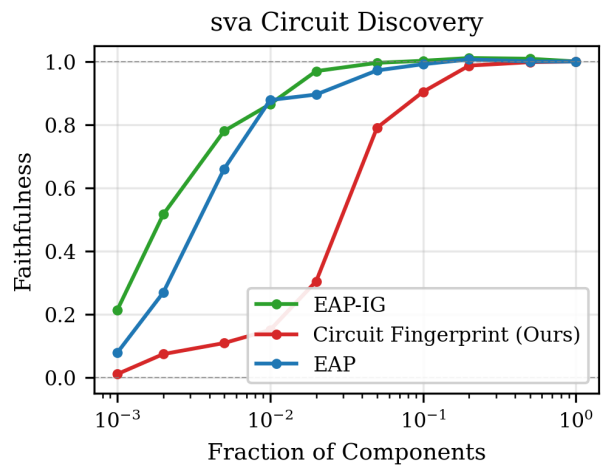
(a) GPT2-Small



(b) Qwen2.5-0.5B



(c) Llama3.2-1B



(d) OPT-1.3B

Figure 8. Edge-level circuit discovery for SVA across models.

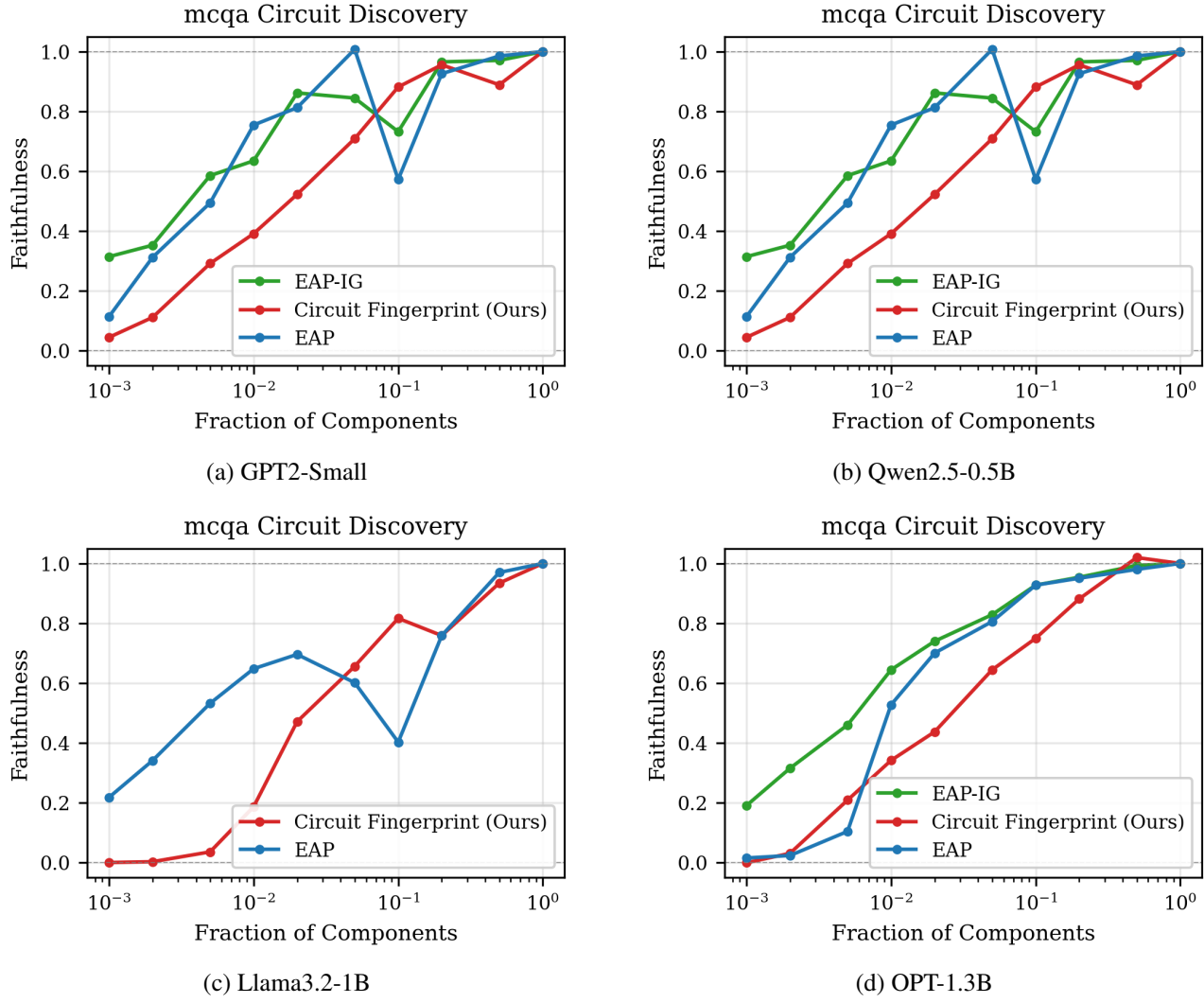


Figure 9. Edge-level circuit discovery for MCQA across models.

B. Activation Patching Comparisson

We present the complete steering validation curves for SVA and MCQA, complementing the IOI results in Figure 5. Both tasks exhibit similar patterns: answer token directions achieve comparable endpoint performance to activation patching despite using only geometric information.

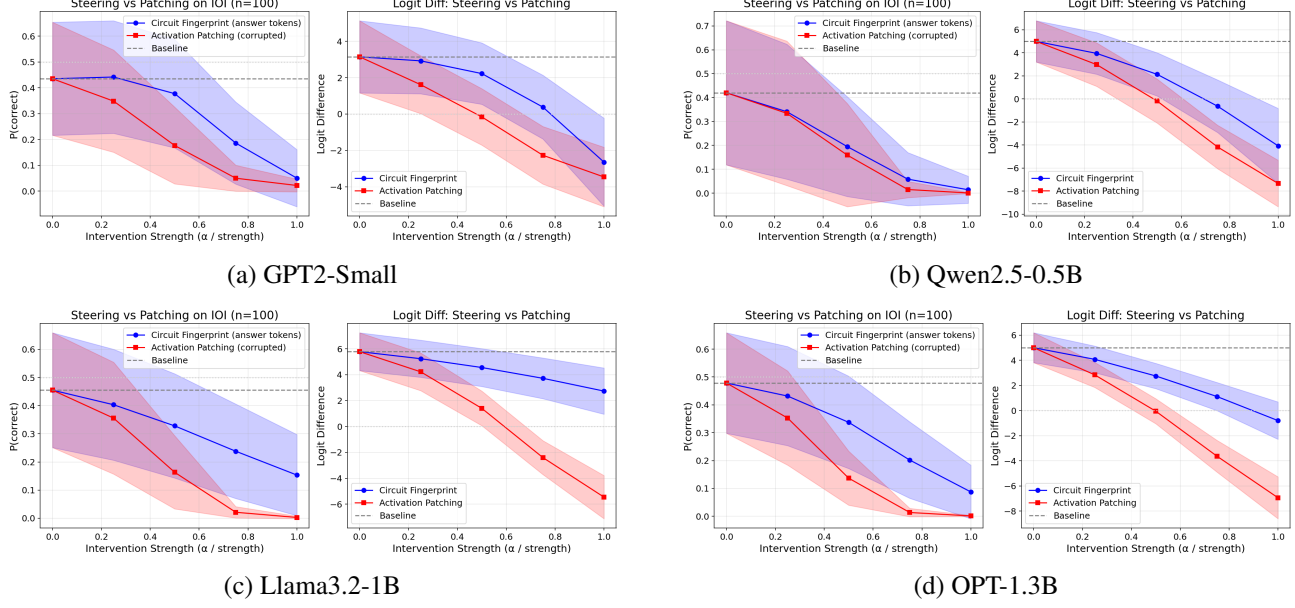


Figure 10. Activation Patching Comparisson for IOI.

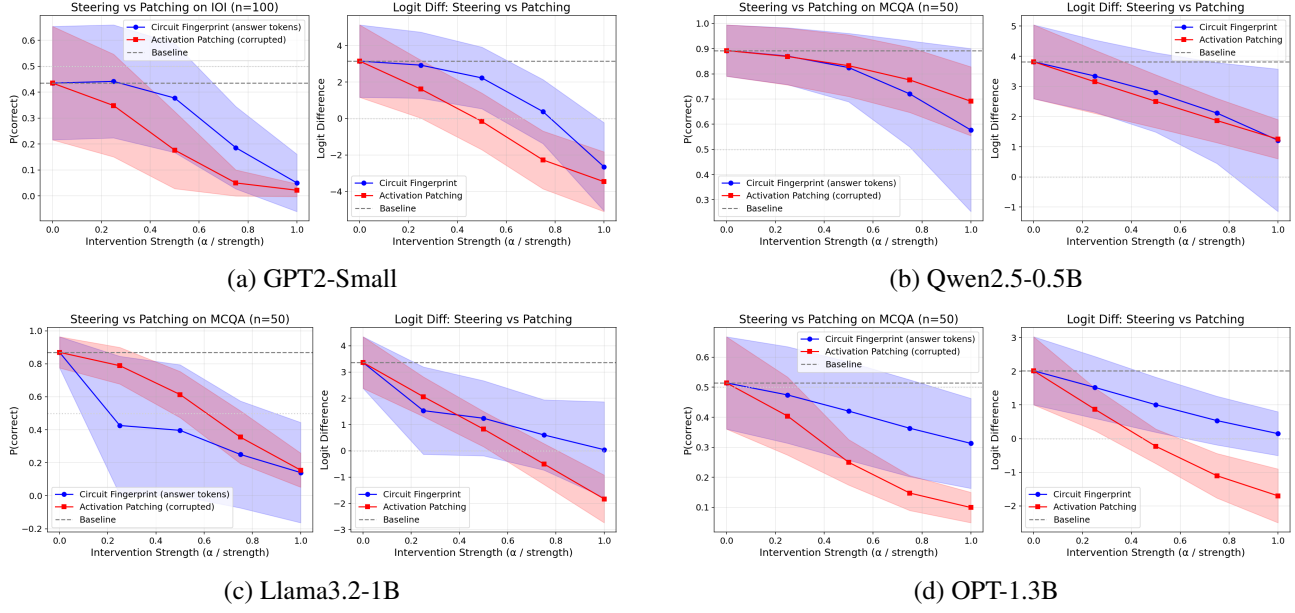


Figure 11. Activation Patching Comparison for MCQA.

C. Steering Class Vectors

Table 4 presents per-emotion results. Geometric steering achieves higher classification accuracy on 3/5 emotions (joy, sadness, surprise), while consistently producing lower perplexity—indicating more fluent generations—without degrading factual accuracy (89.6% vs 90.1%).

Table 4. Per-Language Emotion Steering: Geometric Method vs Instruction Prompting

Emotion	Classification Acc.		Perplexity↓		Factual Acc.
	Baseline	Steered	Baseline	Steered	
Anger	55.1%	24.5%	10.50	11.12	96%
Disgust	75.5%	67.3%	17.95	13.14	78%
Joy	49.0%	87.8%	15.76	12.93	100%
Sadness	53.1%	89.8%	18.09	13.95	81%
Surprise	32.7%	79.6%	22.86	15.72	93%
Average	53.1%	69.8%	17.03	13.37	90%